# Oblique incidence of semi-guided planar waves on slab waveguide steps: effects of rounded edges

## LENA EBERS,* MANFRED HAMMER, AND JENS FÖRSTNER

*Department of Theoretical Electrical Engineering, Paderborn University, Warburger Str. 100, 33098 Paderborn, Germany*
*lena.ebers@uni-paderborn.de

**Abstract:** Oblique propagation of semi-guided waves across slab waveguide structures with bent corners is investigated. A critical angle can be defined beyond which all radiation losses are suppressed. Additionally an increase of the curvature radius of the bends also leads to low-loss configurations for incidence angles below that critical angle. A combination of two bent corner systems represents a step-like structure, behaving like a Fabry-Perot interferometer, with two partial reflectors separated by the vertical height between the horizontal slabs. We numerically analyse typical high-index-contrast Si/SiO$_2$ structures for their reflectance and transmittance properties. When increasing the curvature radius the resonant effect becomes less relevant such that full transmittance is reached with less critical conditions on the vertical distance or the incidence angle. For practical interest 3-D problems are considered, where the structures are excited by the fundamental mode of a wide, shallow rib waveguide. High transmittance levels can be observed also for these 3-D configurations depending on the width of the rib.

## References and links

1. W. Bogaerts, R. Baets, P. Dumon, V. Wiaux, S. Beckx, D. Taillaert, B. Luyssaert, J. Van Campenhout, P. Bienstman, and D. Van Thourhout, "Nanophotonic waveguides in silicon-on-insulator fabricated with CMOS technology," J. Lightwave Technol. **23**(1), 401–412 (2005).
2. R. Soref, "The past, present, and future of silicon photonics," IEEE J. Sel. Top. Quantum Electron. **12**(6), 1678–1687 (2006).
3. P. Prakash Koonath and B. Jalali, "Multilayer 3-D photonics in silicon," Opt. Express **15**(20), 12686–12691 (2007).
4. P. Koonath, T. Indukuri, and B. Jalali, "Monolithic 3-D silicon photonics," J. Lightwave Technol. **24**(4), 1796–1804 (2006).
5. N. Sherwood-Droz and M. Lipson, "Scalable 3D dense integration of photonics on bulk silicon," Opt. Express **19**(18), 17758–17765 (2011).
6. R. A. Soref, E. Cortesi, F. Namavar, and L. Friedman, "Vertically integrated silicon-on-insulator waveguides," IEEE Photonics Technol. Lett. **3**(1), 22–24 (1991).
7. J. K. Doylend, A. P. Knights, C. Brooks, and P. E. Jessop, "CMOS compatible vertical directional coupler for 3D optical circuits," Proc. SPIE **5970**, 59700G (2005).
8. R. Sun, M. Beals, A. Pomerene, J. Cheng, C.-Y. Hong, L. Kimerling, and J. Michel, "Impedance matching vertical optical waveguide couplers for dense high index contrast circuits," Opt. Express **16**(16), 11682–11690 (2008).
9. J. F. Bauters, M. L. Davenport, M. J. R. Heck, J. K. Doylend, A. Chen, A. W. Fang, and J. E. Bowers, "Silicon on ultra-low-loss waveguide photonic integration platform," Opt. Express **21**(1), 544–555 (2013).
10. P. Dong and A. G. Kirk, "Compact grating coupler between vertically stacked silicon-on-insulator waveguides," Proc. SPIE **5357**, 135–142 (2004).
11. J. T. Bessette and D. Ahn, "Vertically stacked microring waveguides for coupling between multiple photonic planes," Opt. Express **21**(11), 13580–13591 (2013).
12. M. Hammer, A. Hildebrandt, and J. Förstner, "Full resonant transmission of semi-guided planar waves through slab waveguide steps at oblique incidence," J. Lightwave Technol. **34**(3), 997–1005 (2016).
13. A. Hildebrandt, A. Alhaddad, M. Hammer, and J. Förstner, "Oblique incidence of semi-guided waves on step-like folds in planar dielectric slabs: Lossless vertical interconnects in 3-D integrated photonic circuits," Proc. SPIE **9750**, 975045 (2016).

14. T. P. Shen, R. F. Wallis, A. A. Maradudin, and G. I. Stegeman, "Fresnel-like behavior of guided waves," J. Opt. Soc. Am. A **4**(11), 2120–2132 (1987).
15. D. N. Chien, K. Tanaka, and M. Tanaka, "Guided wave equivalents of Snell's and Brewster's laws", Opt. Commun. **225**(4), 319–329 (2003).
16. W. Biehlig and U. Langbein, "Three-dimensional step discontinuities in planar waveguides: Angular-spectrum representation of guided wavefields and generalized matrix-operator formalism," Opt. Quantum Electron. **22**(4), 319–333 (1990).
17. S. Misawa, M. Aoki, S. Fujita, A. Takaura, T. Kihara, K. Yokomori, and H. Funato, "Focusing waveguide mirror with a tapered edge," Appl. Opt. **33**(16), 3365–3370 (1994).
18. COMSOL Multiphysics, numerical finite element software, version 5.2. https://www.comsol.de/comsol-multiphysics.
19. L. Ebers, "Oblique semi-guided waves: Modeling quasi-2-D waveguide optics with COMSOL," Master Thesis, Paderborn University, 2017.
20. L. Ebers, M. Hammer, and J. Förstner, "Spiral modes supported by circular dielectric tubes and tube segments," Opt. Quantum Electron. **49**(4), 176 (2017).
21. K. Okamoto, *Fundamentals of Optical Waveguides* (Academic Press, 2000).
22. C. Vassallo, *Optical Waveguide Concepts* (Elsevier, 1991).
23. M. Hammer, "Oblique incidence of semi-guided waves on rectangular slab waveguide discontinuities: A vectorial QUEP solver," Opt. Commun. **338**, 447–456 (2015).
24. K. R. Hiremath, M. Hammer, R. Stoffer, L. Prkna, and J. Čtyroký, "Analytical approach to dielectric optical bent slab waveguides," Opt. Quantum Electron. **37**(1), 37–61 (2005).
25. E. A. J. Marcatili, "Slab-coupled waveguides," Bell Sys. Tech. J. **53**(4), 645–674 (1974).
26. A. G. Rickman, G. T. Reed, and F. Namavar, "Silicon-on-insulator optical rib waveguide loss and mode characteristics," J. Lightwave Technol. **12**(10), 1771–1776 (1994).
27. C. L. Chen, *Foundations for Guided-Wave Optics* (John Wiley and Sons, Inc., 2006).
28. M. Hanke-Bourgeois, *Grundlagen der Numerischen Mathematik und des Wissenschaftlichen Rechnens* (Vieweg+Teubner Verlag, 2008).

## 1. Introduction

Silicon has been one of the pre-eminent materials in the field of integrated optical circuits over the recent decades, because of its compatibility with complementary metal oxide semiconductor (CMOS) technology [1] and the convenient possibility to combine electronic and photonic devices on the same chip [2]. Furthermore new ideas for 3-D integrated platforms with compact, high-index-contrast dielectric optical waveguides at different levels of photonic chips have been introduced [3–5]. Ideally these concepts should work for arbitrary vertical distances with minimal or no power losses. So the question arises which configurations meet the desirable characteristics of a lossless level transfering coupler.

Acceptable results are given by vertically stacked integrated couplers, but these typically require quite large dimensions [6]. A reduction of the height seems feasible only for very low vertical distances [7]. Other concepts make use of coupling through vertically overlapping tapered cores [8, 9], radiative transfer through grating couplers [10] or resonant interaction between vertically stacked microrings [11] to shift power on different levels. But to the best of our knowledge all these structures are either comparably big or suffer from substantial power losses.

Alternatively, in [12, 13] a direct connection between two planar waveguides at different levels by a third vertical waveguide segment was introduced. These structures consist of 90° corners and require comparatively less space. Furthermore it was discovered that for oblique propagation of light and specific vertical distances full transmittance can be achieved by means of exploiting a resonance effect, but the results depend sensitively on the angle and height.

In this paper we want to replace those sharp kinks by slight curvatures, so step-like structures with bent corners like in Fig. 1(b) are investigated for incoming plane waves and oblique angles of incidence. To that end we will consider the configuration from Fig. 1(a) consisting of two vertically connected dielectric slab waveguides with rounded edges, the bent corner structure, at first. Then a corresponding bent step structure like in Fig. 1(b) can be defined as a combination of two of these bent corners and is analysed as well.

Section 2 introduces the theoretical background. A variant of Snell's law applies to those structures and one defines critical angles where radiation losses are suppressed or only a single
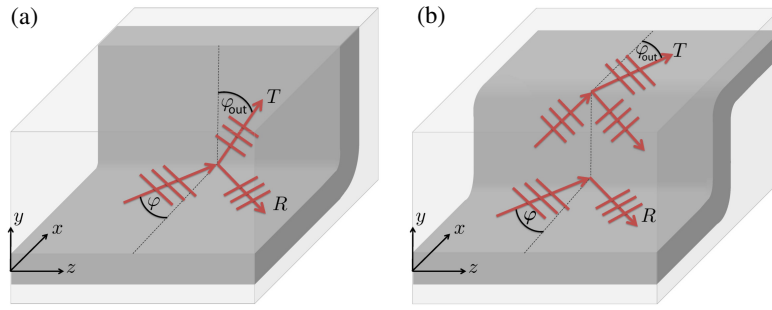
Fig. 1. Bent corner (a) and bent step (b) configuration; oblique wave propagation with incidence angle $\varphi$. Images show incoming, reflected (R) and transmitted (T) waves.

polarisation occurs [14–17]. With the help of the numerical finite element program COMSOL [18] the settings from Fig. 1 are analysed for different incidence angles, curvature radii and vertical step heights. At first the whole structure is assumed to be constant in $z$-direction, which leads to an effective 2-D problem (in the $x$-$y$-plane, with infinite extent in $z$-direction). Afterwards a range of these 2-D solutions is used in Section 3 to assemble 3-D solutions for incoming semi-guided laterally limited wave bundles as can be excited through shallow rib waveguides.

Corner and step structures with sharp edges were analysed with semi-analytical methods in [12] with the same high-index-contrast waveguide parameters as used in this paper, such that the previous models can be compared directly to the present numerical results. We could numerically verify the formal semi-analytical prediction [19]. The investigation of curved structures is also of great interest for the realization of these concepts, because inaccuracies during the fabrication may lead to rounding of the critical edges. We shall see that the present structure with rounded edges can actually be advantageous, e.g. what concerns fabrication tolerances, through weakening the conditions on the aforementioned resonance effect.

## 2. Oblique wave propagation along bent slab waveguide corners

At first we consider a quasi-2-D setting, meaning all structures are infinitely extended in $\pm z$-direction, starting with the bent corner configuration from Fig. 2(a). Here, two half-infinite dielectric slab waveguides with the same core thickness $d$ are connected vertically by a rounded edge with outer curvature radius $r$. The slab waveguide parallel to the $x$-axis is leading the incoming wave and possible reflected waves in -$x$-direction. The second slab waveguide, parallel to the $y$-axis, guides the transmitted waves that have passed the curved segment.

Alternative curvature definitions are possible as well, e.g. configurations with equal radii of the inner and outer interfaces. But that definition leads, in certain circumstances, to strong resonant effects with maximal reflection for specific incidence angles as shown in [19]. Such a behaviour is not useful for the present context, it even gives detrimental results. Hence, we will focus on the parametrization from Fig. 2. Here, the curved part, of constant thickness $d$, was already analysed for guided modes in [20] and similarities in field pattern could be observed [19].

We assume that the structures only guide the fundamental modes, the $TE_0$ and $TM_0$ modes with effective indices $N_{TE_0}$ and $N_{TM_0}$. Furthermore the incoming wave is always the $TE_0$ mode. All relevant fields have a harmonic time dependence $\sim e^{i\omega t}$ with angular frequency $\omega = k_0 c_0 = 2\pi c_0/\lambda_0$, for vacuum wavenumber $k_0$, vacuum speed of light $c_0$, and vacuum wavelength $\lambda_0$.

Considering the incoming oblique wave at first, a field dependence $\sim \exp(-i(k_x x + k_z z))$ applies to all field components. The wave is propagating in the $x$-$z$-plane (see Fig. 2) under an incidence angle of $\varphi$ with wavenumbers $k_z = k_0 N_{TE_0}\sin\varphi$ and $k_x = k_0 N_{TE_0}\cos\varphi$, which
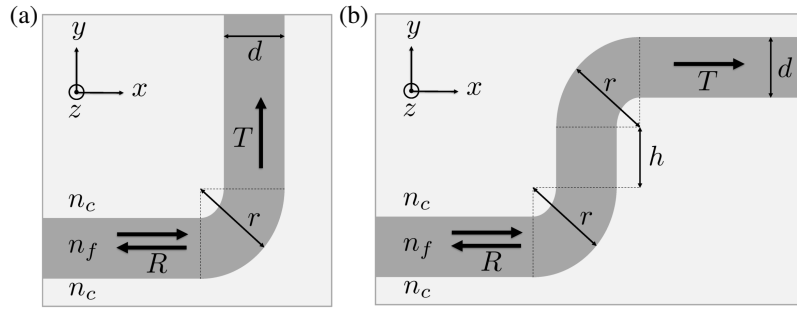
Fig. 2. Cross section of the bent corner (a) and bent step (b) configuration with refractive index $n_f = 3.4$ in the core and $n_c = 1.45$ in the claddings, thickness $d = 0.25\mu m$ and vacuum wavelength $\lambda_0 = 1.55\mu m$. Incidence angle $\varphi$, vertical step height $h$ and curvature radius $r$ are variable parameters.

fulfil the relation $k_0^2 N_{TE_0}^2 = k_x^2 + k_z^2$ as known from the planar slab waveguide [21, 22]. Because of the homogeneity of the waveguide in $z$-direction, the wavenumber $k_z$ applies to the entire electromagnetic field solution. So for the outgoing waves a dependence of $\sim \exp(-i(k_z z + k_\xi \xi))$ describes the fields, where the wave is propagating in the $\xi$-$z$-plane with wavenumber $k_\xi$ in some direction $\xi$. Here, we have $\xi = y$ for the transmitted waves, $\xi = -x$ for the reflected waves and for any scattering wave $\xi$ is a suitable direction in the $x$-$y$-plane.

The relation $k_0^2 N_{out}^2 = k_z^2 + k_\xi^2$ determines the wavenumber $k_\xi$ for the outgoing waves with effective refractive index $N_{out}$. Two cases have to be distinguished. Either $N_{out}$ is sufficiently large and fulfils $k_0^2 N_{out}^2 > k_z^2$, so the waves are propagating at an outgoing angle $\varphi_{out}$, which is defined by a variant of Snell's law $N_{out}\sin\varphi_{out} = N_{TE_0}\sin\varphi$, or $N_{out}$ is small with $k_0^2 N_{out}^2 < k_z^2$ and the outgoing fields become evanescent. Referring to that, a critical angle can be defined by $\sin\varphi_{crit} = N_{out}/N_{TE_0}$ beyond which all power transfer to that particular outgoing wave is suppressed. For the considered Si/SiO$_2$ index contrast a critical angle $\varphi_c = 30.45°$ can be determined by the ratio $\sin\varphi_c = n_c/N_{TE_0}$, where all radiation losses are suppressed in the claddings and everything is guided in the core. An additional angle $\varphi_m = 51.14°$ is defined by $\sin\varphi_m = N_{TM_0}/N_{TE_0}$. Beyond that critical angle all the power is carried by TE$_0$ modes, because the TM$_0$ mode has an effective mode index below $N_{TE_0}$.

In a next step we will analyse these 2-D corner structures governed by the Maxwell's equations with the help of the finite element software COMSOL Multiphysics [18]. Here, port boundary conditions and perfectly matched layer (PML) are the crucial boundary conditions used in this work. Ports are able to excite and absorb plane waves of a known shape and direction and to directly calculate S-parameters. With the help of a numerical 'Boundary Mode Analysis' solver the corresponding modes to excite the structures are calculated. PMLs are used to simulate infinite space and open boundaries by absorbing all types of outgoing waves without reflections. Furthermore the considered structures are analysed in a 2-D environment by defining an out-of-plane wavenumber $k_z$ to simulate oblique incidence. To verify the program settings, 2-D structures, already analysed with semi-analytical methods [12, 20, 23, 24], were investigated [19]. We observed an excellent agreement of our numerical solutions with the existing results.

## 2.1. Bent corners

First the bent corner structure from Fig. 2(a) is analysed. Figure 3 shows the numerical transmittance and reflectance values, concerning the fundamental guided modes, for different curvature radii $r$ as a function of the incidence angle $\varphi$. The calculations were carried out for refractive indices $n_f = 3.4$ in the core and $n_c = 1.45$ in the claddings, core thickness $d = 0.25\mu m$,
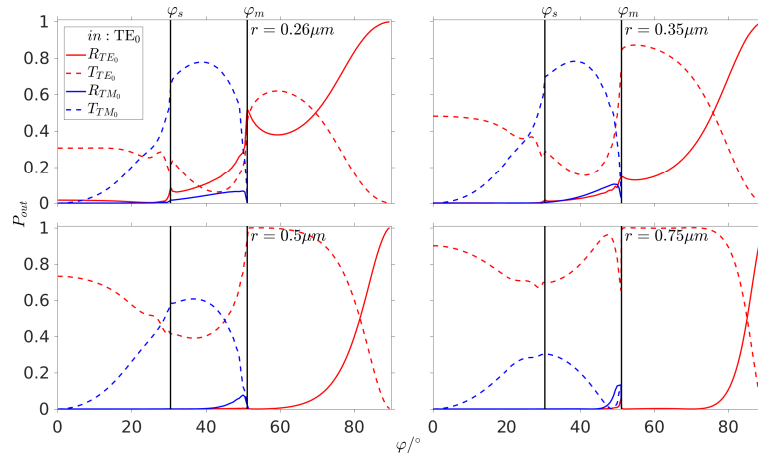
Fig. 3. Transmittances $T_{TE_0}$, $T_{TM_0}$ and reflectances $R_{TE_0}$, $R_{TM_0}$ of the bent corner structure depending on the incidence angle $\varphi$ for different curvature radii $r$.
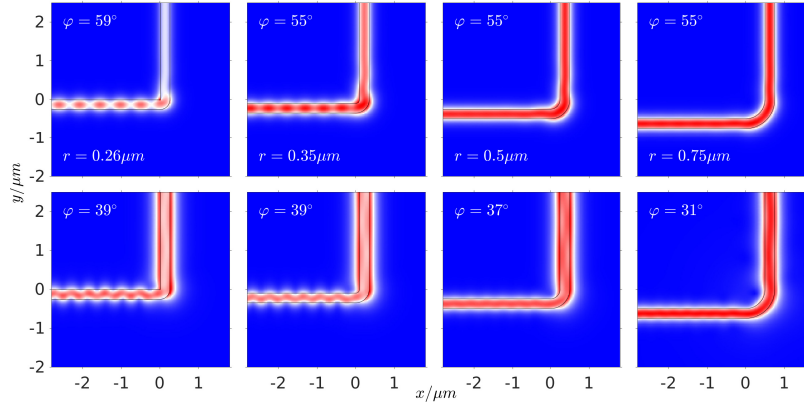


Fig. 4. Absolute electric field $|\mathbf{E}|$ for the bent corner structure for different radii and angles of incidence with maximal TE transmittance (upper row) and maximal TM transmittance (bottom row).

at a typical near-infrared wavelength $\lambda_0 = 1.55\mu m$ for incidence of the $TE_0$ wave.

Referring to the defined critical angles radiation losses occur for incidence angles smaller $\varphi_c$, meanwhile beyond that angle everything is guided by reflected or transmitted TE and TM waves. As expected, for waves propagating at an incidence angle higher than $\varphi_m$ no power is carried by outgoing TM waves and only propagating TE waves leave the structure. In general, for increasing curvature radius the reflectance of both, TE and TM polarized waves, tend to zero and the transmittance enhances. The TE reflectance value only increases rapidly for grazing incidence, at angles close to $90°$. Furthermore the transmittance levels of the TM polarized waves decrease for an increasing radius, so the polarization conversion becomes less.

Figure 4 shows corresponding field plots of the absolute electric field $|\mathbf{E}|$ for angles with maximal TE and TM transmittance. One notices less guided wave reflectance in the incoming slab for increasing curvature radius in both rows. Already from these results it can be concluded that a raised curvature radius leads to improved transmission properties.

## 2.2. Bent steps

In a next step we combine two of the former bent corner structures. The bent step structure of Fig. 2(b) consists of two horizontal waveguides and a connecting vertical segment, all of identical thickness. This represents the actual structure of interest for power transfer between various heights. A new variable parameter appears, the vertical distance between the parallel slabs $h$ according to Fig. 2(b).

The waveguide parameters are still the same as in Section 2.1 and therefore the critical angles are also identical. Thus we will only focus on the lossless cases, which means incidence angles higher than $\varphi_c = 30.45°$. More precisely we analyse the step structure for variable vertical step heights $h$, with curvature radius $r$ and incidence angle $\varphi$ fixed at the selected values from Fig. 4, where the corner structure shows maximal TE and TM transmittance.
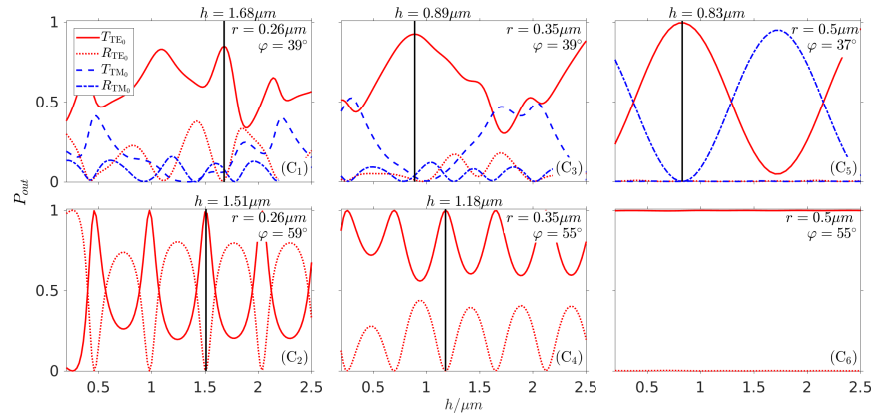


Fig. 5. Transmittances $T_{TE_0}$, $T_{TM_0}$ and reflectances $R_{TE_0}$, $R_{TM_0}$ of the bent step structure depending on the vertical distance $h$ for specified incidence angles $\varphi$ and curvature radii $r$ from the corner structure in Section 2.1. Vertical lines indicate heights with maximal transmittance that are selected for the plots of Figs. 6–7.
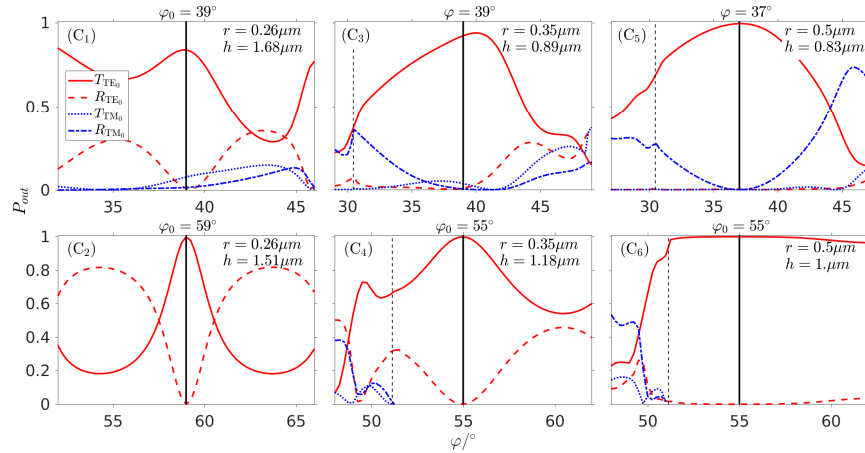


Fig. 6. Transmittances $T_{TE_0}$, $T_{TM_0}$ and reflectances $R_{TE_0}$, $R_{TM_0}$ of the bent step for different incidence angles $\varphi$ around the primary incidence angle $\varphi_0$ for specific radii $r$ and heights $h$.

Figure 5 shows the transmittance and reflectance depending on the step height $h$ for fixed radius and angle. Since the differences between $r = 0.5\mu m$ and $r = 0.75\mu m$ are not very significant we

will only focus on radii up to $0.5\mu m$ in the following. Considering a small curvature radius of $r = 0.26\mu m$ and a large angle of $\varphi = 59°$ (see config. ($C_2$)), this means a structure where only TE waves occur, one notices a strong periodic behaviour between reflected and transmitted TE waves. Such an appearance was also discovered in [12, 13] and is due to a resonant effect between the two horizontal slabs, where upward and downward propagating waves are present in the vertical segment. This effect can be compared to a Fabry-Perot interferometer, where the corners play the role of the partial reflectors. By scanning over the vertical distance $h$ full transmission appears for certain equidistant heights. Next considering for equal curvature radius a smaller incidence angle $\varphi = 39°$ (see config. ($C_1$)) the oscillating behaviour becomes less regular. This is because both polarisations, TE and TM waves, mediate in the vertical waveguide segment. For larger curvature radii, as can be seen for config. ($C_3$)–($C_6$), the before observed periodic behaviour becomes less pronounced with wider peaks. The modulation of transmittance levels reduces up to almost full transmittance regardless of the vertical step height and occurring polarisation ($C_6$). Additionally Fig. 6 shows the transmittance and reflectance for varying incidence angle around a primary angle $\varphi_0$. An increase in bend radius is seen to reduce the angular dependence, the transmittance maxima widen for lower curvature. In Section 3 this angular dependence becomes relevant for the 3-D solutions.
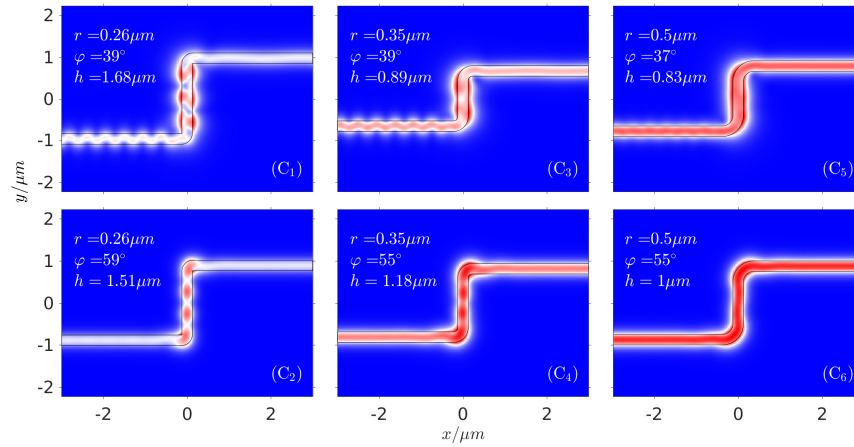


Fig. 7. Absolute electric field $|\mathbf{E}|$ for bent step structures for different radii, heights and angles of incidence with maximal TE transmittance from Fig. 5.

To illustrate the height dependence of the steps Fig. 7 shows the 2-D field plots of the absolute electric field $|\mathbf{E}|$ for specific angles and radii from Fig. 5 and heights with high TE transmittance as also marked in Fig. 5. As already stated, for small radii counter propagating waves interfere in the vertical waveguide segment. For higher radii these interference pattern disappear.

## 3. Laterally guiding step configurations in 3-D

The previous quasi-2-D results concern oblique incoming semi-guided waves that are infinitely extended along the $z$-direction. Now we want to consider more practially relevant true 3-D solutions as well. We investigate laterally limited wave bundles as incoming waves in those structures. Such limited modes can be excited by using rib waveguides [25, 26] as seen in Fig. 8(a). We assume a wide rib width $l$ of thickness $d$ with shallow etching depth of $d' = 0.01\mu m$ to guarantee lateral guidance and avoid to much spreading of the wave packets in the adjoining slab.

When connecting an incoming rib waveguide to a slab, as shown in Fig. 8(a), a wave that is guided by the rib waveguide and limited in the lateral direction can be expected to remain reasonably limited after entering the slab waveguide. Here, the junction is shown in rotated
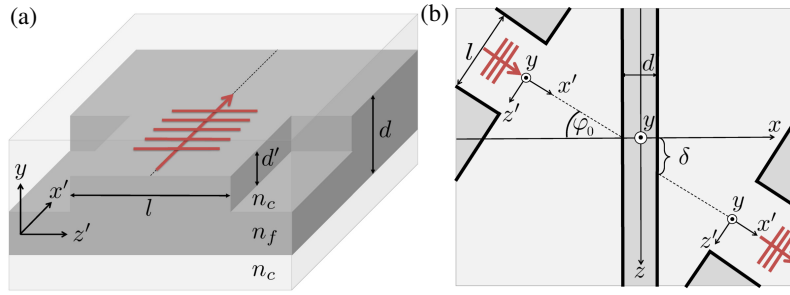
Fig. 8. Connection of a rib and slab waveguide (a) of thickness $d$ with refractive indices $n_f$, $n_c$ in rotated coordinates $(x', y, z')$. In (b) the view from above for incoming and outgoing waves under primary incidence angle $\varphi_0$ is shown. The ribs have a width of $l$ and an etch depth of $d' = 0.01\,\mu m$; other parameters are as given for Fig. 2.

coordinates $(x', y, z')$, where the $x'$-direction is parallel to the waveguide axis, i.e. parallel to the propagation direction of the incoming mode under incidence angle $\varphi_0$. So using this configuration our structure of interest, the bent step, is excited by a laterally confined wave. A second identical rib is placed at the end of the step structure (see Fig. 8(b)) to catch the transmitted power. The displacement $\delta$ between the axes of the incoming and outgoing ribs is related to the vertical propagation through the step (marked by the grey bar in the middle of Fig. 8(b)) and will be selected depending on the vertical height. Similarly, the distance between the step and the rib waveguide is reasonably adjusted depending on the rib width so that back reflections do not touch the incoming rib.

The underlying theoretical approach to calculate 3-D solutions was introduced by the authors in [12] for incoming Gaussian wave packets. However, exciting the structure by a rib waveguide appears to be more realistic and is therefore considered in the following theoretical approach. At the outset it should be noted that possible back reflections at the transitions between the rib and the slab waveguides are neglected. Then a 3-D wave bundle for incoming primary incidence angle $\varphi_0$ is given by a superposition of weighted 2-D solutions for a range of wavenumbers $k_z$ (or incidence angles $\varphi$) around the primary wavenumber $k_{z_0}$ (or primary incidence angle $\varphi_0$) [12] and is evaluated by

$$\begin{pmatrix} \mathbf{E} \\ \mathbf{H} \end{pmatrix}(x, y, z) = A \int_{-\infty}^{\infty} w(k_z)\{\mathbf{\Psi}_0(k_z, y)e^{-ik_x(k_z)(x-x_0)} + \boldsymbol{\rho}\}e^{-ik_z(z-z_0)}dk_z. \tag{1}$$

Here, $w(k_z)$ is a weighting function determined by the incoming laterally guided mode of the rib waveguide. The term in curly brackets depicts the former quasi-2-D solution in the $x$-$y$-plane evaluated in COMSOL with the vectorial profile $\mathbf{\Psi}_0$ for incoming oblique $TE_0$ incidence and a remainder $\boldsymbol{\rho}$. The last phase factor represents the individual harmonic $z$-dependences of the elementary quasi-2-D solutions. Offsets $x_0$, $z_0$ have been introduced to normalize the global phase of the bundle to the end facet of the incoming waveguide. Finally $A$ is the amplitude of the fields.

To evaluate the unknown weight $w(k_z)$ the guided mode profile of the etched rib waveguide, given in local coordinates $(x', y, z')$ and calculated in COMSOL with the 'Mode Analysis' solver, is transformed to the global coordinates $(x, y, z)$. For simplicity the following calculations are shown for normal incidence only, so $(x, y, z) = (x', y, z')$. To determine the unknown weight $w(k_z)$ the mode profile $\mathbf{\Phi}_0$ of the fundamental quasi-TE mode of the rib can be written as a superposition of the complete set of normal modes $\mathbf{\Psi}_j$ supported by the slab waveguide at the junction plane where rib and slab waveguides meet,

$$\mathbf{\Phi}_0(y, z) = A \sum_j \int_{-\infty}^{\infty} w_j(k_z)\mathbf{\Psi}_j(k_z, y)e^{-ik_z(z-z_0)}dk_z, \tag{2}$$

where $j$ identifies mode orders. Using the complex product

$$(\mathbf{\Psi}, \mathbf{\Phi})_y := \frac{1}{4} \int_{-\infty}^{\infty} (E_{1y}^* H_{2z} - E_{1z}^* H_{2y} + H_{1z}^* E_{2y} - H_{1y}^* E_{2z}) \mathrm{d}y \tag{3}$$

defined for mode orthogonality with the transverse field components of two different modes $\mathbf{\Phi} = (\mathbf{E_1}, \mathbf{H_1})$ and $\mathbf{\Psi} = (\mathbf{E_2}, \mathbf{H_2})$ [27] and assuming that the modes are orthogonal and power normalized the unknown weight is given by

$$w_0(k_z) = \frac{1}{2\pi A} \int_{-\infty}^{\infty} (\mathbf{\Psi}_0, \mathbf{\Phi}_0)_y \mathrm{e}^{ik_z(z-z_0)} \mathrm{d}z. \tag{4}$$

By rotating the coordinates and fields by the appropriate angle, so transforming $\mathbf{\Psi}_j(y)$ from the global to the local coordinate system, the desired calculation can also be made analogously for oblique incidence.

After passing the discontinuity we want to catch the TE$_0$ mode back again in a rib with identical width $l$, so the field profiles of incoming and outgoing wave are identical except for a pre-factor $u_0 \in \mathbb{C}$ that represents the transmission coefficient. The outgoing field profile $\mathbf{\Psi}_{\mathrm{out}}(y, z)$ can again be expressed as a superposition of all existing modes in the rib waveguide $\mathbf{\Phi}_j(y, z)$, which leads to

$$\mathbf{\Psi}_{\mathrm{out}}(y, z) = \sum_j u_j \mathbf{\Phi}_j(y, z). \tag{5}$$

Once again by applying the product for mode orthogonality [27], now for two transverse coordinates, with $\mathbf{\Phi} = (\mathbf{E_1}, \mathbf{H_1})$ and $\mathbf{\Psi} = (\mathbf{E_2}, \mathbf{H_2})$ given by

$$(\mathbf{\Phi}, \mathbf{\Psi})_{y,z} := \frac{1}{4} \int_{-\infty}^{\infty} \int_{-\infty}^{\infty} (E_{1y}^* H_{2z} - E_{1z}^* H_{2y} + H_{1z}^* E_{2y} - H_{1y}^* E_{2z}) \mathrm{d}y \mathrm{d}z, \tag{6}$$

and assuming mode orthogonality and power normalization, here for the modes of the rib waveguide, Eq. (5) leads to the resulting complex transmission coefficient

$$u_0 = (\mathbf{\Phi}_0, \mathbf{\Psi}_{\mathrm{out}})_{y,z}. \tag{7}$$

The integrals in Eqs. (1), (4), (7) required to calculate the 3-D solutions were evaluated using numerical quadrature [28]. Here, the range of superimposed angles and the step size play an important role for the accuracy of the results. Note that quadrature parameters required for convergence depend on the spectral properties of the expanded fields, i.e. the rib width.

As for the structure with sharp edges [12], the beam width, here determined by the width $l$ of the rib, is very important to guarantee acceptable field properties. In general, for a small rib width, a wide range of incidence angles has influence on the field properties and vice versa. At this point we refer to Fig. 6 in order to clarify the angular dependence of these 3-D structures. For small curvature radii slight changes in the incidence angle lead to larger changes in transmittance and reflectance values (see config. (C$_1$), (C$_2$)). Thus, small, sharper bends require large widths to avoid influence of unintended back reflections. However, the rib width can be reduced for increased bend radius (config. (C$_3$)–(C$_4$)), because the angular dependence of the step transmittance becomes less intense. So increasing the radius results in a decrease of the necessary rib width that leads to acceptable field properties.

### 3.1.    3-D solutions

Some resulting 3-D fields are shown in Fig. 9 for incidence angles, curvature radii and vertical distances as analysed for the 2-D case in Fig. 7.

The rib widths $l$ were selected such that the wave bundles showed neither pronounced additional reflections when compared to the 2-D situation, nor substantial spreading. For the
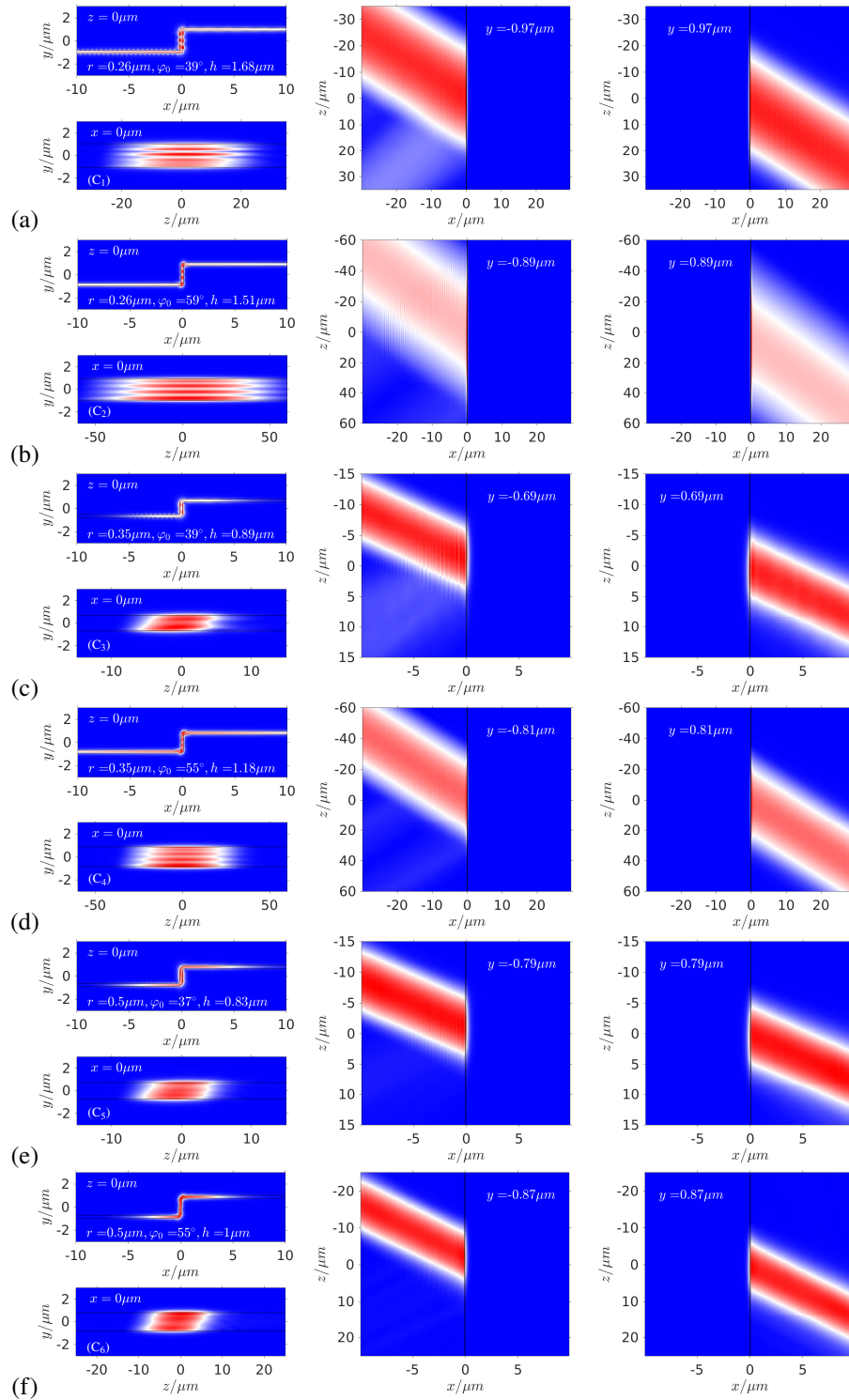
Fig. 9. Electric field $|\mathbf{E}|$ for incidence of laterally guided modes for the bent step structure for different radii $r$, primary angles $\varphi_0$ and heights $h$ as used before in Fig. 7 for rib widths (a) $l = 40\mu m$, (b) $l = 60\mu m$, (c) $l = 10\mu m$, (d) $l = 40\mu m$ (e) $l = 10\mu m$, (f) $l = 10\mu m$.

present parameters used below, we observe hardly any divergence of the wave bundles excited by the incoming rib mode. The small image on the upper left shows the field properties of the cross section in the $x$-$y$-plane, the lower left image represents the field in the vertical segment in the $z$-$y$-plane, and furthermore the middle and right images demonstrate the absolute field value of the electric field in the horizontal plane for the incoming wave (middle) and transmitted wave (right) in the $x$-$z$-plane with a view from above. Note that only the fields in the infinite slab waveguide step are shown without the incoming rib.

As expected, small to no reflectance can be observed for large radii, while for small radii the reflected waves are still present. Furthermore for increasing radius a much smaller rib width $l$ is required down to a comparably narrow width of $10\mu m$ for configuration ($C_6$) (see Fig. 9(f)). For the structures with sharp edges in [12] large beam widths up to $180\mu m$ were necessary to avoid unintentional reflections. So the bent structures provide better field properties for narrow incoming wave bundles.

### 3.2.  Power transmittance

In a last step we look at the transmittance levels for the $TE_0$ mode in the previous 3-D steps. According to the formulas of Section 3, the TE transmittance (see Eq. (7)) is directly given by the coefficient $|u_0|^2$. Results for the structures of Section 3.1 are shown in Fig. 10. In addition to the previously considered curved configurations ($C_1$)–($C_6$), the calculations were also carried out for steps with sharp edges ($S_1$), ($S_2$) from [12]. The rib widths for these structures are adopted from the bent structures with smallest curvature radius (config. ($C_1$) and ($C_2$)), meanwhile the incidence angles $\varphi = 41°$ and $\varphi = 68°$ are taken from the results in [12] and correspond to maximal transmittance in 2-D.
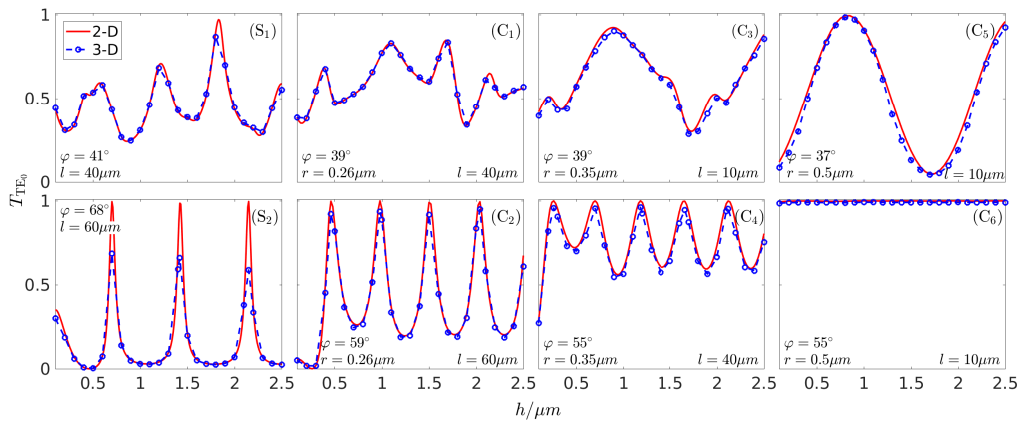


Fig. 10. $TE_0$ transmittances for the 3-D (blue line) bent step structure (config. ($C_1$)–($C_6$)) and sharp step structure (config. ($S_1$)–($S_2$)) from [12], for incoming and outgoing rib of width $l$, depending on the height $h$ for different incidence angles and radii. The red line refers to the corresponding 2-D results from Section 2.1, with laterally unlimited incoming waves.

The continuous blue line in Fig. 10 shows the 3-D TE transmittance values for incoming $TE_0$ mode for specified rib widths $l$ as used before in Section 3.1, whereas the dashed red line illustrates the corresponding 2-D TE transmittances from Section 2.1. For the structure with sharp edges the 2-D transmittances were also determined with COMSOL. The configurations for the sharp structure, especially ($S_2$), require a large rib width to achieve comparable results to the 2-D calculations. In [12], it was already shown that beam widths up to $180\mu m$ were necessary to guarantee acceptable field behaviour for these $90°$ structures.

Referring to the bent structures there is no perfect agreement with the 2-D results, because the

angular dependence has huge influence on the field properties, but the results show quite good agreement. Therefore the excitation of 3-D bent step structures with the help of a rib waveguide is a practical possibility and leads to excellent transmittance values.

## 4. Conclusion

With the help of the numerical finite element software COMSOL Multiphysics, bent corner and step structures were investigated. Optical quasi-2-D and 3-D scattering problems in the frequency domain were solved. By changing the incidence angle, the curvature radius and the vertical step height, configurations with high transmittance values could be identified. The following behaviour applies to these bent structures: For large radii the incoming wave is nearly completely transmitted for arbitrary incidence angles and height, while for small radii substantial reflections are observed. Here, only for specific heights and incidence angles full transmittance is reached. A resonance effect, similar to a Fabry-Perot-Etalon, was observed, when scanning over the step height.

Finally, laterally confined 3-D solutions were considered, where the structures were excited by the fundamental mode of a wide, shallow rib waveguide. Solutions are calculated as a superposition of 2-D solutions for a range of propagation angles. One obtains wave packets of a specific width for a defined primary angle. With the help of a second outgoing rib waveguide, transmittance values for the 3-D structure could be calculated. In general, for adjusted rib widths, the results show good agreement with the transmittance values for the effective 2-D structures. For low curvature radii a large rib width is necessary, because only wavevectors that fulfil the resonant condition lead to correct field properties. By increasing the curvature radius also smaller widths lead to high transmittance values, here the resonant effect has less influence. So for practical interest such bent structures can yield a high level of transmission with comparably small laterally widths.

Consequently, it was shown that energy transfer to different levels, in 3-D integrated optical chips, by using bent slab waveguides might be a promising, practically relevant concept. By increasing the curvature radius the transmittance levels become even almost completely independent of the incidence angle or step height.